3-D crustal *P*-wave velocity tomography of the Italian region using local and regional seismicity data

Bruno Alessandrini, Laura Beranzoli and Francesco M. Mele
Istituto Nazionale di Geofisica, Roma, Italy

Abstract
A tomographic experiment was performed in the Italian region using local and regional arrival times of *P* and *S* seismological phases selected from the Italian National Bulletin in the time interval 1984-1991. We determined a 3-D crustal *P*-wave velocity model using a simultaneous inversion method that iteratively relocates the hypocenters and computes the unknown model parameters. A fast two-point ray tracing algorithm was adopted to compute the ray paths and travel times of P_n, S_n, P_g, S_g phases with good accuracy. Synthetic tests were performed using the «true» hypocenter and station distribution to roughly evaluate the extension of the areas most densely spanned by the ray paths; the agreement between synthetic and computed models is more satisfactory at Moho depths than in the upper crust. The quality of the model resulting from inversion of real data is examined by the calculation of the Spread Function (Toomey and Foulger, 1989). The 3-D crustal *P*-wave velocity model of the Italian region shows remarkable trends at Moho depths: the areas east of the Apennines call for positive adjustments of the initial velocity value, while the west region shows negative adjustments. The correspondence among the main features of the velocity field, the map of Moho isobaths and the map of the gravity anomalies is also outlined.

Key words *inversion algorithms – seismic tomography – Moho structure*

1. Introduction

The structure of crust and upper mantle of the Italian area has been studied by many authors applying various techniques making use of both seismological data and geophysical exploration data. Teleseismic body wave arrival times have been used to define the gross structure of crust and upper mantle of the Earth since the early Seventies. Scarpa (1982) used the ACH method (Aki *et al.*, 1977) to estimate the extent of the velocity contrast in the Central Mediterranean area. Strong lateral variations on horizontal scale of about 50 to 100 km characterize the lithosphere in the Italian region up to 5 to 10%. The Italian peninsula was the object of other inversions of teleseismic arrival times, covering the whole of Western Europe (Romanowicz, 1980; Babuška *et al.*, 1984a,b). More detailed studies were performed by Amato *et al.* (1991, 1993); these authors applied the ACH method as modified by Ellsworth and Koyanagi (1977) and Evans (1986), to a selected set of *P* and *PKP* digital waveforms recorded by the short-period Italian National Seismographic Network (hereafter referred to as INSN) of the Istituto Nazionale di Geofisica (ING). Although some models presented by Amato *et al.* (1993) have thickness of 30 km for the uppermost layer, teleseismic travel times tomography gives poor resolution

in the crust. The steepness of incident rays limits the resolution to a narrow cone underneath the seismological station, and the crustal and upper mantle structure is weakly constrained by the data. The large scale *P*-wave velocity structure of the upper mantle beneath Europe, the Mediterranean Sea and South-West Asia, including the Italian peninsula, was analyzed by Spakman (1986, 1990) using tomographic inversion of ISC-delay times from about 30000 regional events. The adopted model consisted of blocks with horizontal dimension of 100 km and vertical dimension ranging from 33 km to 130 km.

Calcagnile and Panza (1981) analyzed Rayleigh wave dispersion data for the Italian area in the ranges 40 to 150 s. The inversion of these data showed strong lateral variations in the lithosphere system.

Mantovani and Boschi (1982) investigated crustal structure and lateral heterogeneities of the Central Mediterranean area by studying Rayleigh wave dispersion in the period range 5-35 s. They drew a dispersion curve for the Adriatic platform (toponyms are mapped in fig. 1) typical of a stable continental structure

Fig. 1. Toponyms used for the Italian region.

with no low velocity channel. A possible similar structure was inferred for in the Po Valley covered by a sedimentary layer of more than 10 km. Moreover the upper sedimentary layer in the southern part of the Apennines seems to be thinner than in the northern part. The dispersion curve of the Southern Tyrrhenian Sea indicates a thinned layer of crustal material and a possible soft lithospheric mantle. In the Ionian Sea the dispersion curve indicates a crust of intermediate or continental type. Mantovani *et al.* (1985) studied short period Rayleigh wave dispersion and found a continuous structure extending from North Africa through the Ionian Sea to the Adriatic Sea, indicating the continental nature of the crust in this area, with a high velocity layer below the Moho; they also found a crustal thickness in the range 32 to 38 km beneath the Apennines, 28 to 32 km in the Adriatic plate, 27 to 51 km in the volcanic area extending from Tuscany to Campania, 35 to 40 km in the Po Valley and 15 to 20 km in the Southern Tyrrhenian Sea.

During the last four decades many studies of Deep Seismic Sounding (DSS) profiles have been performed in Italy. Some authors (Nicolich, 1981; Cassinis, 1983; Cassinis and Ranzoni, 1987; Nicolich, 1989) attempted to give a comprehensive interpretation of such data. Nevertheless the information from DSS data cannot easily be used to define a model for earthquake location procedures. Some detailed 3-D crustal models have been derived in areas of limited size where dense networks were installed (Amato *et al.*, 1990).

Mantovani *et al.* (1980) analyzed the velocity of compressional and shear body-waves from local earthquakes in the Italian peninsula and surrounding areas. The velocities of P_g, P_n, S_g and S_n waves were determined dividing the area into laterally homogeneous regions, and inverting travel time residuals of about 3500 ray paths. A decrease in P_n and S_n velocities going from the Adriatic to the Tyrrhenian region was also shown. They found P_g and P_n velocity values in the range 5.6 to 6.0 km/s and 7.6 to 8.2 km/s respectively. Mele and Valensise (1987) investigated the *P*-wave velocity field at the Moho and the thickness of the crust, inverting about 6300 P_g and P_n arrival

times in a regionalized model in which each region was considered laterally homogeneous. They found an average Moho depth of 41 km and an average P_n velocity of 8.08 km/s. They pointed out the presence of a high velocity zone (8.0-8.2 km/s) in the uppermost mantle that extends through the Adriatic Sea and the Po Valley, and a lower velocity (7.6-8.0 km/s) in the western volcanic area and the Tyrrhenian Sea.

In this work we estimate the *P* velocity in the crust and in the crust-mantle transition zone (Moho) using earthquake arrival times of P_g, S_g, P_n and S_n phases recorded by the INSN of the ING and by other Italian and foreign seismological networks. We applied an inversion method, as described by Pavlis and Booker (1980) and modified by Thurber (1983) consisting of the simultaneous determination of the 3-D *P*-wave velocity field and relocation of events via an iterative scheme. A starting model was adopted assigning velocity values at each node of a 3-D grid with a prefixed v_p/v_s ratio. The theoretical travel times and residuals were computed using the ray tracing technique by Prothero *et al.* (1988).

2. Data description

The data set used in the tomographic experiment consisted of arrival times of events extracted from the seismological bulletin of the ING. The bulletins were drawn up after the analysis of digital seismic signals recorded by the short period seismometers of INSN, by smaller Italian networks and by other regional and national networks of neighbouring countries. We performed an initial selection on the original data base accepting only seismic events occurred within 40 km of depth in the geographical area extending 36°N to 48°N of latitude and 6°E to 20°E of longitude.

As the methodology required well constrained event locations, that is low rms of residuals (Thurber, 1983), the earthquakes selected were relocated using the HYPOINVERSE algorithm (Klein, 1978) in a laterally homogeneous layered model and the same model was successively used as a starting model for the inversion (see section 4). Because of the trade-off between the error due to mislocations and the error induced by the poor knowledge of the true model, well constrained locations of the events are required in order to obtain reliable results. Therefore we accepted only events with at least 20 *P*-wave arrival times whose rms of residuals did not exceed 1.5 s; in our case that was almost the same as selecting events with a magnitude larger than about 3.

The final data set consisted of 22430 arrival times (65% P_n, 17% P_g, 3% S_n and 15% S_g) corresponding to 419 events and 309 seismological stations. The small amount of *S* arrival times, dramatically decimated in the selection process, is explained by the usually greater inaccuracy of their readings with respect to *P* arrival times and the consequently larger residual values associated with the location algorithm.

The maps in fig. 2a,b show respectively stations and epicenters included in the data set; the projection at the surface of the ray path coverage of the studied area for *P* and *S* waves are shown in fig. 2c,d. The Italian Peninsula and the Adriatic Sea are crossed by many ray paths while wide areas of the Tyrrhenian basin are not well «illuminated» by the rays. 84% of the events have a number of observed phases ranging from 30 to 70. Most of the events have a number of P_n and S_n arrival times ranging respectively from 30 to 60 and from 0 to 30. The contribution of P_g and S_g arrival times to the data set is below P_n and S_n (about one third of the total) because of the seismological station coverage.

3. Method

Given a starting estimation of velocity structure $v(x, y, z)$, hypocenter coordinates and origin time of each earthquake, the residual r^{ik} corresponding to the *i*-th observation (receiver) and the *k*-th earthquake is defined as

$$r^{ik} = T^{ik}_{obs} - T^{ik}_{cal} \qquad (3.1)$$

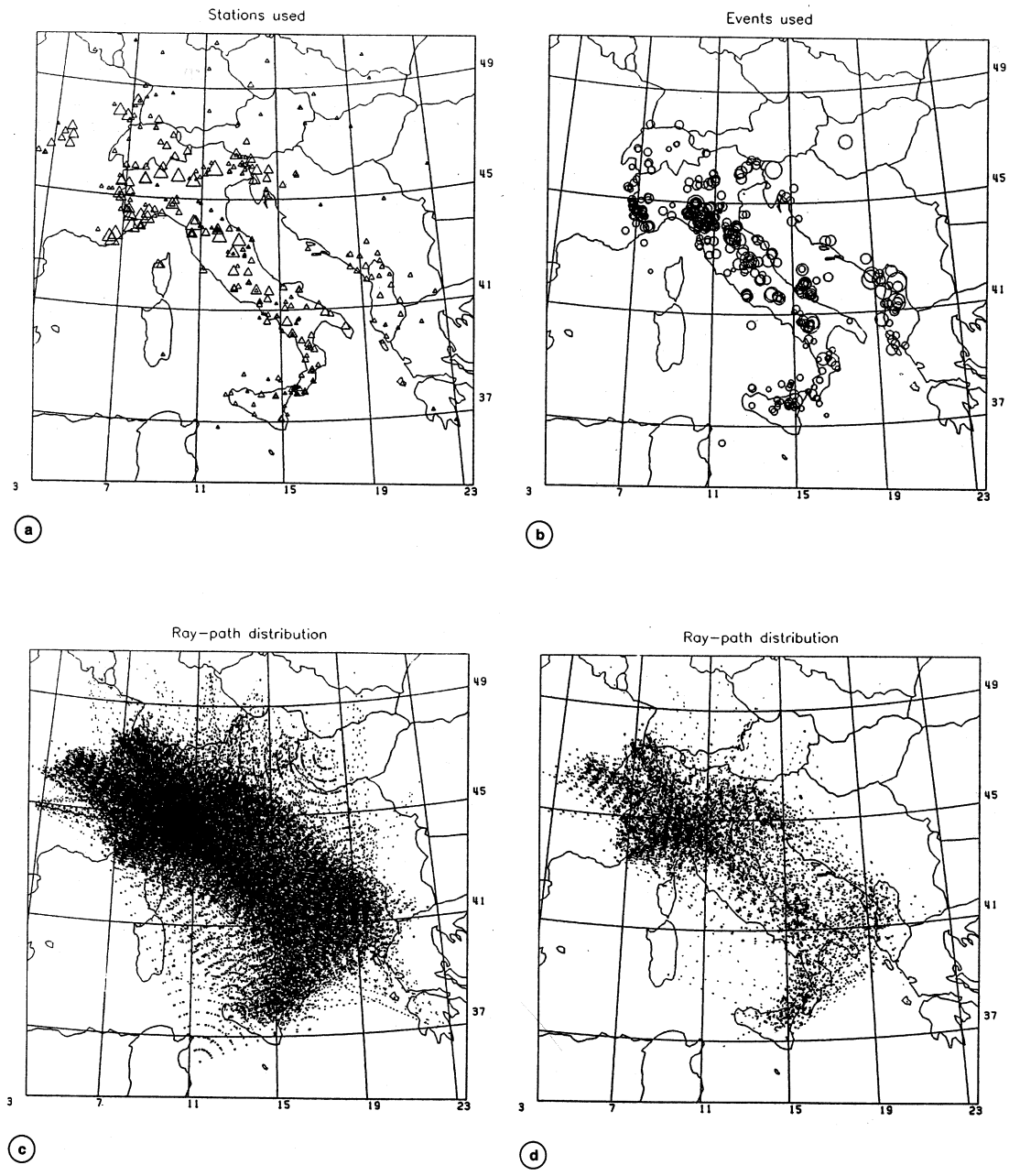

Fig. 2a-d. Station (a) and epicenter distribution (b); symbol size is proportional to the number of arrival times observed. Ray path coverage for *P* (c) and *S* waves (d).

where T^{ik}_{obs} is the i-th observed travel time and T^{ik}_{cal} is the i-th travel time computed using a ray tracing algorithm. For each r^{ik} the following linearized equation is set (Thurber, 1981):

$$r^{ik} = \Delta t_o^k + \frac{\partial T^{ik}}{\partial x_e^k}\Delta x_e^k + \frac{\partial T^{ik}}{\partial y_e^k}\Delta y_e^k + \frac{\partial T^{ik}}{\partial z_e^k}\Delta z_e^k + \sum_{j=1}^{N}\frac{\partial T^{ik}}{\partial v_j}\Delta v_j \qquad (3.2)$$

where $\frac{\partial T^{ik}}{\partial x_e^k}$, $\frac{\partial T^{ik}}{\partial y_e^k}$, $\frac{\partial T^{ik}}{\partial z_e^k}$ are the partial derivatives of the travel time with respect to the epicenter coordinates, $\frac{\partial T^{ik}}{\partial v_j}$ are the partial derivatives of the travel time with respect to the j-th model parameter, N is the total number of model parameters, Δt_o^k, Δx_e^k, Δy_e^k, Δz_e^k and Δv_j are the unknown adjustments of the hypocentral and model parameters. The set of eq. (3.2) can be written in matrix form:

$$A\underline{x} = \underline{r} \qquad (3.3)$$

where A is the known matrix of partial derivatives, $\underline{r}$ is the known vector of residuals and $\underline{x}$ is the unknown vector of parameter adjustments. Many observations are usually required to obtain the ray path coverage of the studied area as dense as possible and the size of the matrix A, which depends on both the number of model parameters and the number of observations, can pose many difficulties in solving eq. (3.3).

The method developed by Pavlis and Booker (1980) and modified by Thurber (1983) overcomes that drawback with the separation of the hypocenter part of the matrix from the model part for each earthquake (parameter separation); as a consequence, the size of the matrix to be inverted is fixed by the number of model parameters only. The hypocentral partial derivatives depend on the velocity at the source and the initial direction of the ray path, while the type of parameterization and the interpolation function used for the velocity model play a major role in the computation of the partial derivatives of travel times with respect to the velocity parameters (Thurber, 1983).

In this study the model parameterization consisted of a 3-D grid of nodes, each with an assigned velocity value; the velocity v in an arbitrary location (x, y, z) is given by the following linear interpolation function:

$$\begin{aligned} v = {} & [(x_{i+1}-x_i)(y_{j+1}-y_j)(z_{k+1}-z_k)]^{-1} \\ & [(x_{i+1}-x)(y_{j+1}-y)(z_{k+1}-z)\,v_{i,j,k} \\ & +(x-x_i)(y_{j+1}-y)(z_{k+1}-z)\,v_{i+1,j,k} \\ & +(x_{i+1}-x)(y-y_j)(z_{k+1}-z)\,v_{i,j+1,k} \\ & +(x-x_i)(y-y_j)(z_{k+1}-z)\,v_{i+1,j+1,k} \\ & +(x_{i+1}-x)(y_{j+1}-y)(z-z_k)\,v_{i,j,k+1} \\ & +(x-x_i)(y_{j+1}-y)(z-z_k)\,v_{i+1,j,k+1} \\ & +(x_{i+1}-x)(y-y_j)(z-z_k)\,v_{i,j+1,k+1} \\ & +(x-x_i)(y-y_j)(z-z_k)\,v_{i+1,j+1,k+1}] \end{aligned} \qquad (3.4)$$

where x_i, x_{i+1}, y_j, y_{j+1}, z_k and z_{k+1} are the coordinates of the nodes surrounding the point of coordinates (x, y, z) and $v_{i,j,k}$ is the velocity at the generic grid point.

The travel times were computed through the two-point 3-D ray tracing algorithm by Prothero *et al.* (1988), which has the advantage of being extremely fast. The first step of this algorithm consists in searching the circular arc connecting the source and the receiver site that minimizes the travel time. The selected circular arc is then perturbed by sine harmonics expansion with coefficients computed via the Simplex Method (Nelder and Mead, 1965). A good accuracy in refracted ray paths is available using 9 harmonics. Figure 3 shows two vertical cross sections with some ray paths in the distance range 8 to 670 km computed in the starting model used in the inversion of the real data for two hypocenters at 5 and 20 km of depth. This approximation technique is a good com-

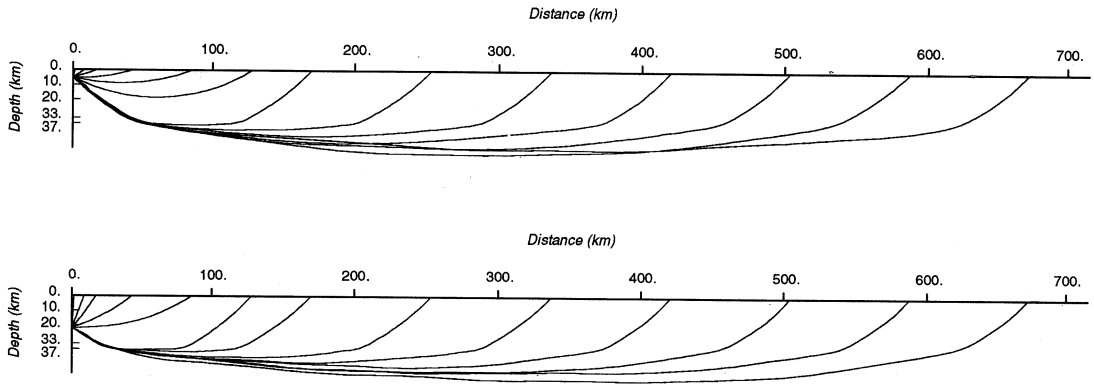

Fig. 3. Vertical cross sections with ray paths in the distance range 8 to 670 km computed in the starting model used in the inversion of the real data for two hypocenters at 5 and 20 km of depth.

promise between computation speed and solution accuracy; for more details see the original paper by Prothero *et al.* (1988).

The iterative approach proposed by Thurber (1981) may be outlined by the following scheme:

a) calculation of theoretical arrival times in the starting 3-D discretized velocity model, via two-point 3-D ray tracing, and calculation of partial derivatives;

b) separation of velocity parameters from hypocentral parameters via QR decomposition and consequent determination of a new data vector $\underline{r}'$ and a matrix M', whose elements are hypocentral-independent velocity partial derivatives;

c) solution of the hypocentral-independent system of equations

$$M'\underline{\Delta v}' = \underline{r}' \qquad (3.5)$$

with respect to the adjustments of the velocity parameters $\underline{\Delta v}'$ using

$$\underline{\Delta v}' = [(M')^T M + \varepsilon^2 I]^{-1} (M')^T \underline{r}' \qquad (3.6)$$

where ε is a damping factor;

d) updating of the model parameters;

e) relocation of the earthquakes separately with 3-D ray tracing and arrival time calculation in the adjusted velocity model; a new matrix A is computed;

f) restart from point b).

4. Data inversion

Because of the linearization set in eq. (3.2) the final velocity model was expected to be close to the starting model. So the choice of the latter had to be made accurately. Our starting model was defined on the basis of the studies previously described in the introduction (Mantovani *et al.*, 1980; Mele and Valensise, 1987). The model was parameterized assigning *P*-wave velocity values to a finite set of nodes in a 3-D Cartesian coordinate system.

The Moho depth undergoes considerable variations in the studied area, ranging from 40-50 km below the Alps to less than 20 km in the Southern Tyrrhenian Sea (Nicolich and Dal Piaz, 1990). It is easily verified that a variation of the crustal thickness affects the travel time of a wave refracted at the Moho mostly in its crustal path. In a simple scheme of a flat Moho dipping 10 km in a horizontal distance of 100

km, the path length under the crust experiences a variation, with respect to a horizontal Moho, of less than 0.5 km (less than 0.07 s at 8.0 km/s), while more than 1.4 s are required to cross the additional 10 km of crust with a vertical path at 7.0 km/s. As a consequence when velocities at the Moho are sufficiently constrained by the data the largest errors in travel time computation, are caused by the crustal terms. Although a residual bias between poor modeling of the crustal thickness and velocity values found at the Moho cannot be excluded, we nevertheless argue that a simplified scheme is sufficient to point out some main features of the velocity field in the upper mantle. Our starting model consisted of four flat crustal layers bounded by five grids of nodes located at 0, 10, 20, 33 and 37 km of depth. In our starting reference model the velocities assigned to the nodes belonging to the five grids were 5.6, 6.0, 6.5, 7.0 and 8.1 km/s respectively; variations to these values were the unknown parameters of the model. A grid of nodes at 220 km of depth, at a fixed velocity of 8.5 km/s, bound our model to the upper mantle, while another grid at 10 km over sea level, with a fixed velocity of 4.8 km/s, was used to take into account station elevations. The velocity in the starting model was, in each layer, a linear function of depth only.

The velocity increment from 7.0 to 8.1 km/s within 4 km of thickness at the bottom of the crust has been set in order to model the crust-mantle transition zone.

The independence of the results from the node spacing was verified adopting two different 3-D grids of nodes. The first (model 1) was composed of horizontal grids of 21×23 nodes spaced 52 km in the E-W direction and 60 km in the S-N direction. A second one (model 2) was composed of a smaller number of nodes (11×13 per layer) and a larger sampling space (100 km both in the E-W and N-S directions). A rough picture of models 1 and 2 is shown in fig. 4a,b. A finer sampling of the crustal volume under investigation was prevented by the memory size of the computer used.

During the ray tracing computation, the number of rays passing near each node was counted. Velocity variations were computed only for nodes contributing to the computation of at least 10 ray paths. The number of nodes

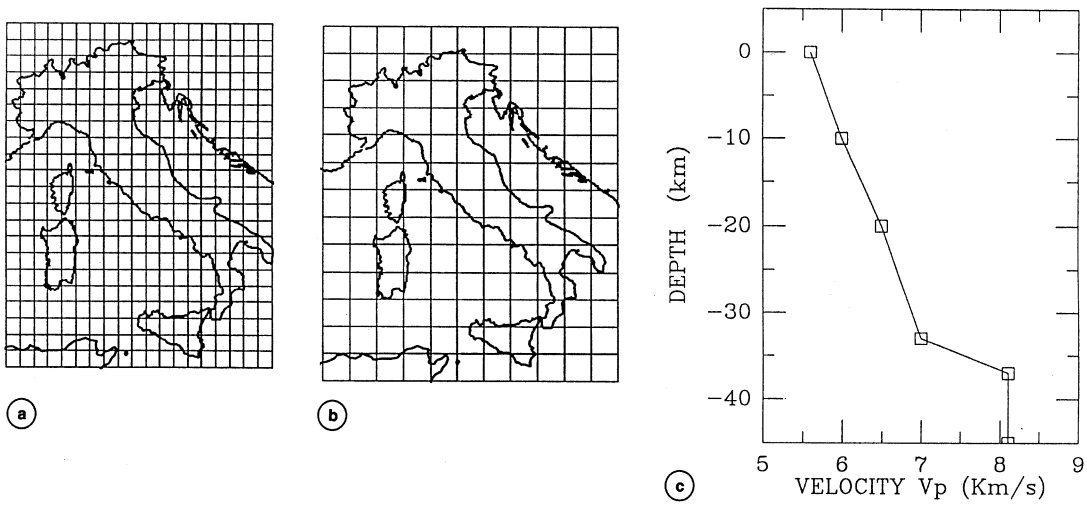

Fig. 4a-c. Top view of the horizontal grid of 21×19 nodes (a) (excluding boundary nodes which were held fixed) and of the grid of 13×11 nodes (b) superimposed on the geographical map of the investigated area; c) starting V_p velocity model.

of model 1 whose velocity values were really inverted was reduced to 1380.

As previously mentioned, a large portion of the selected data set came from recordings made by the digital acquisition system of the ING at a sampling rate of 50 sps. Hence uncertainty on selecting impulsive P phase could be as low as 0.02 s. Unfortunately, this condition seldom came true; moreover part of our data set came from various other Italian and foreign seismological networks, in some cases they are still not equipped with digital acquisition devices, with possible inconsistencies in reference times. Therefore we assigned to all P phases an *a priori* standard deviation of 0.2 s. The number of available S arrival times was not sufficient to invert for both P and S velocities in each node. Figure 5 shows the selected P and S wave travel-time picks T as a function of epicenter to receiver distance Δ. We approximated the data distribution with linear functions of the form $T = \tau + \sigma \cdot \Delta$, where τ is a time and σ is the phase slowness in distance ranges of 200 km, and we found the apparent P and S velocity values shown in table I.

The apparent velocity ratio V_P/V_S is almost constant in the epicenter-receiver distance range 0 to 600 km. As the inclusion of S information from a theoretical point of view vastly improves the reliability of the locations (Buland, 1976), we decided to use the S phases available in the data set with an epicenter-station distance not exceeding 600 km, assuming a constant V_P/V_S ratio of 1.73. We assigned to all the S phases an *a priori* standard deviation of 1.6 s.

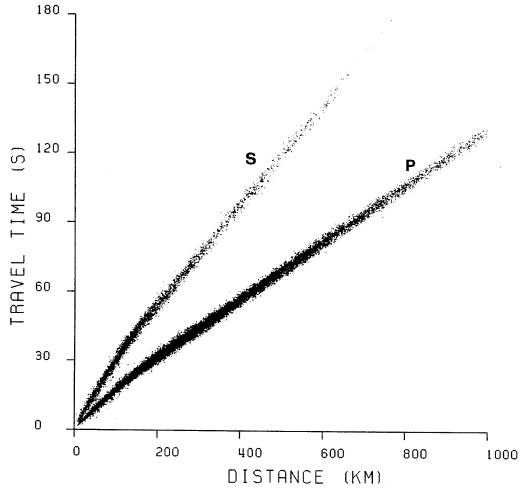

Fig. 5. Travel times for P and S waves from the data set used for the inversion. V_p/V_s may be estimate by the slopes of the P and S trends.

Table I. Apparent P and S velocity values for different hypocenter-receiver distances obtained from travel times of our data set. The ratio V_p/V_s is also reported.

Δ (km)	V_p (km/s)	V_s (km/s)	V_p/V_s
0-200	6.40	3.75	1.73
200-400	7.92	4.56	1.74
400-600	8.09	4.68	1.73
600-800	8.15	4.35	1.87

At each iteration of the inversion procedure the data were weighted with a function $w = w_1 \cdot w_2 \cdot w_3$, where w_1 is the reciprocal of the *a priori* standard deviation and w_2 was defined as follows for a phase recorded at an epicentral distance Δ:

$$w_2 = 1 ; \qquad \Delta < d_1 \tag{4.1}$$

$$w_2 = 0 ; \qquad \Delta > d_2 \tag{4.2}$$

$$w_2 = \frac{1}{2} \cdot \left[1 - \cos\left(\pi \frac{\Delta - d_2}{d_1 - d_2} \right) \right] ; \qquad d_1 \leq \Delta \leq d_2 \tag{4.3}$$

d_1 is 200 km for all the phases; d_2 is 1000 km for P phases and 600 km for S phases. w_3 is a function of the residual associated to the phase; it is equal to 1 for phases with residual not exceeding 1.5 s, is 0 for phases with residual exceeding 3 s. For residual values ranging 1.5-3 s, w_3 followed a cosine function of the residual as shown in eq. (4.3).

A series of inversions to determine the best value to attribute to the damping were exe-

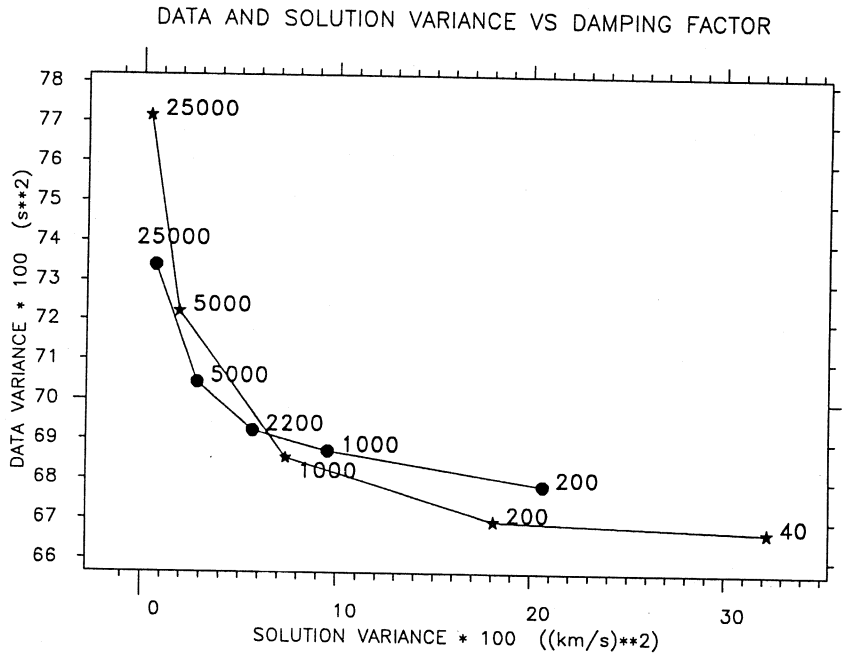

Fig. 6. Trade-off curve of model and data variance for the finer grid size (★), and less dense grid (●).

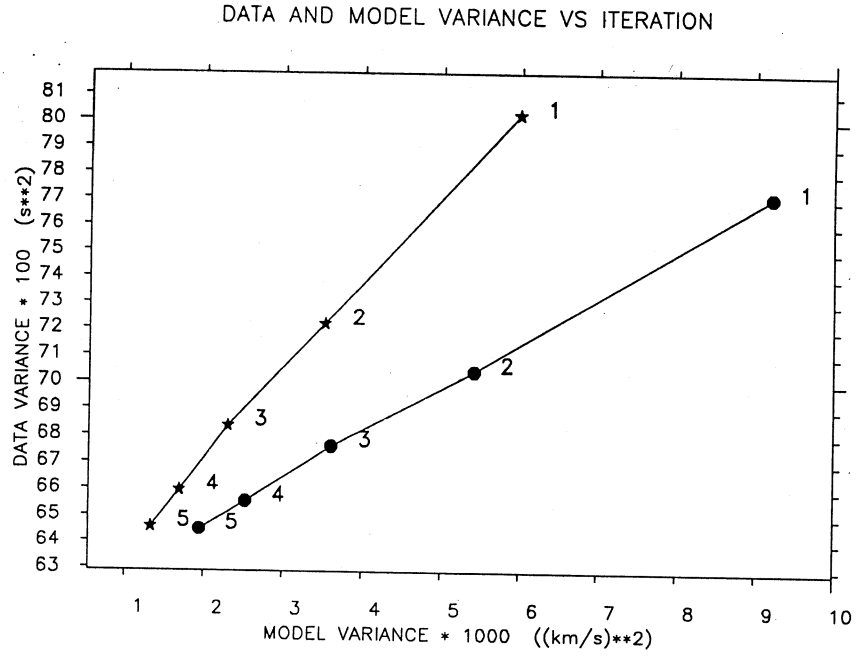

Fig. 7. Data variance and model variance vs iterations for the finer grid size (★), and less dense grid (●).

cuted. Trade-off curves for both models of residual data variance versus damping factor after two iterations are depicted in fig. 6. A damping factor around 5000 was the best compromise between data and solution variance for both models. In the inversion of the real data, a damping factor of 5000 was assumed and iterations were performed until the ratio of two successive residual variances fell below a critical value defined by an F test (Menke, 1984). The plot of residual variance and solution variance versus number of iterations is shown in fig. 7; solution variances were computed with respect to the model obtained in the previous iteration. From fig. 7 one can conclude that the variance reduction was not significant after the fifth iteration for both models 1 and 2.

5. Synthetic tests

The accuracy in the estimate of velocity anomalies in a given zone is a function of the density of ray paths sampling that zone. We performed synthetic simulations using the hypocenter and station distribution of the actual data set, in order to check qualitatively which parts of the studied area are better spanned by the rays.

Synthetic paths and travel times were computed with the same 3-D ray tracing technique used in the inversion procedure. Random normally distributed errors with zero mean and standard deviation of 0.2 s were added to the computed travel times P. The errors added to the S travel times had a standard deviation of 1.6 s. A first test was performed imposing a model S_c, laterally heterogeneous in the upper crust (from 0 to 20 km of depth) and laterally homogeneous in the lower crust and upper mantle. In a second test a model S_m was set laterally heterogeneous in the upper mantle and homogeneous in the crust. Sketches of the models S_c and S_m are shown in fig. 8b,c. In both cases the chosen velocity field consisted of a sequence of blocks with high and low velocity values and rectangular shape (hereafter called the *checkerboard model*). Figure 8a shows the map view of the variable part of the test models. The mean velocity value of each layer was assigned as in fig. 4c; the variable part of the models S_c and S_m had velocity anomalies of $\pm$ 5% with respect to the mean value.

The results of the synthetic test are shown in figs. 9 and 10. Percent variations of the velocity with respect to starting values are reported: blue areas correspond to higher positive velocity adjustments, gray areas correspond to not-inverted nodes due to lack of ray paths. Inverting the data set produced with model S_m, we argue that at Moho depths the velocity is better constrained in the Adriatic region and below the Italian peninsula while the velocity heterogeneities are completely hidden below the Tyrrhenian Sea (see fig. 9). In this area two types of ray paths are mostly observed: from hypocenters in Sicily to receivers located in Northern Italy, and *vice versa.* Both these types of ray paths are almost parallel, so that it is impossible to discriminate velocity values at different nodes. This can be done for the nodes hit by crossing ray paths: under the INSN and the Adriatic Sea the checkerboard model is better reproduced because of the presence of ray paths both with north-south and east-west direction.

Some major difficulties arise in the estimate of velocity anomalies in the upper crust inverting data produced with model S_c (fig. 10). The crustal volume sampled by the rays under each receiver is cone shaped, with the vertex coinciding with the receiver site; the shallower the layer investigated, the smaller the volume spanned by the seismic rays. Moreover the ray direction under the station is nearly vertical, so that lateral velocity variations cannot be investigated in all those areas with a poor station coverage. Therefore, in the inversion of real data, we expected reliable results in the peninsular crust and at the Moho.

6. Solution quality

A measure of quality includes the estimate of data variance reduction and model resolution (Menke, 1984). The data variance is a measure of the disagreement between observed and predicted data; in our case the data vari-

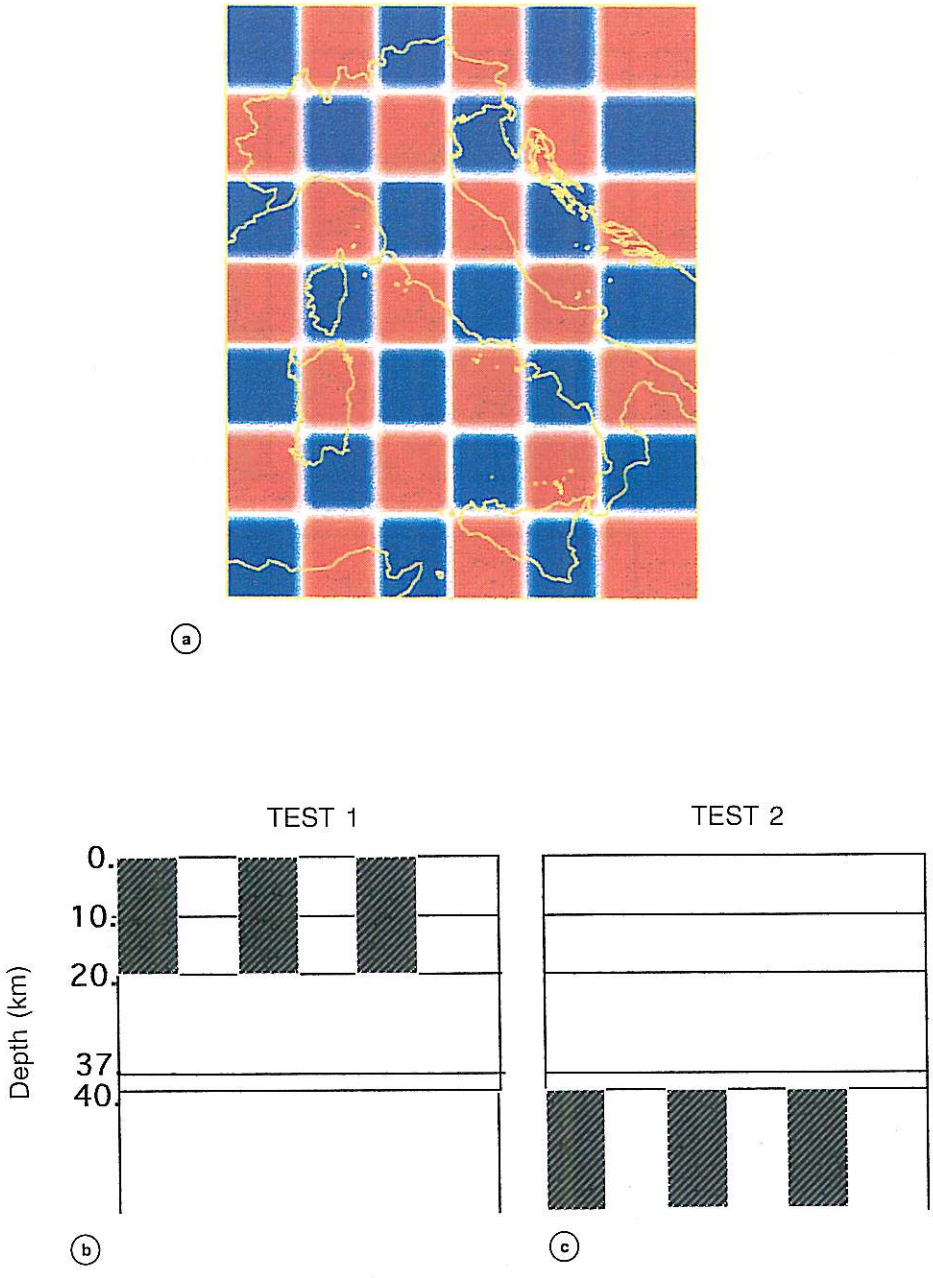

Fig. 8a-c. Sketches of the S_c and S_m models used for the synthetic tests. a) Map view of the variable part of both S_c and S_m test model. The horizontally homogeneous layers extend under 20 km of depth for the S_c test model (b) and from 0 to 40 km of depth in the S_m test model (c); the variable part is confined from 0 to 20 km of depth in the S_c model and under 40 km of depth for the S_m model. The shaded and white blocks correspond to V_p values of 6.1 and 5.5 km/s in the S_c model and to 8.4 and 7.6 km/s in the S_m.

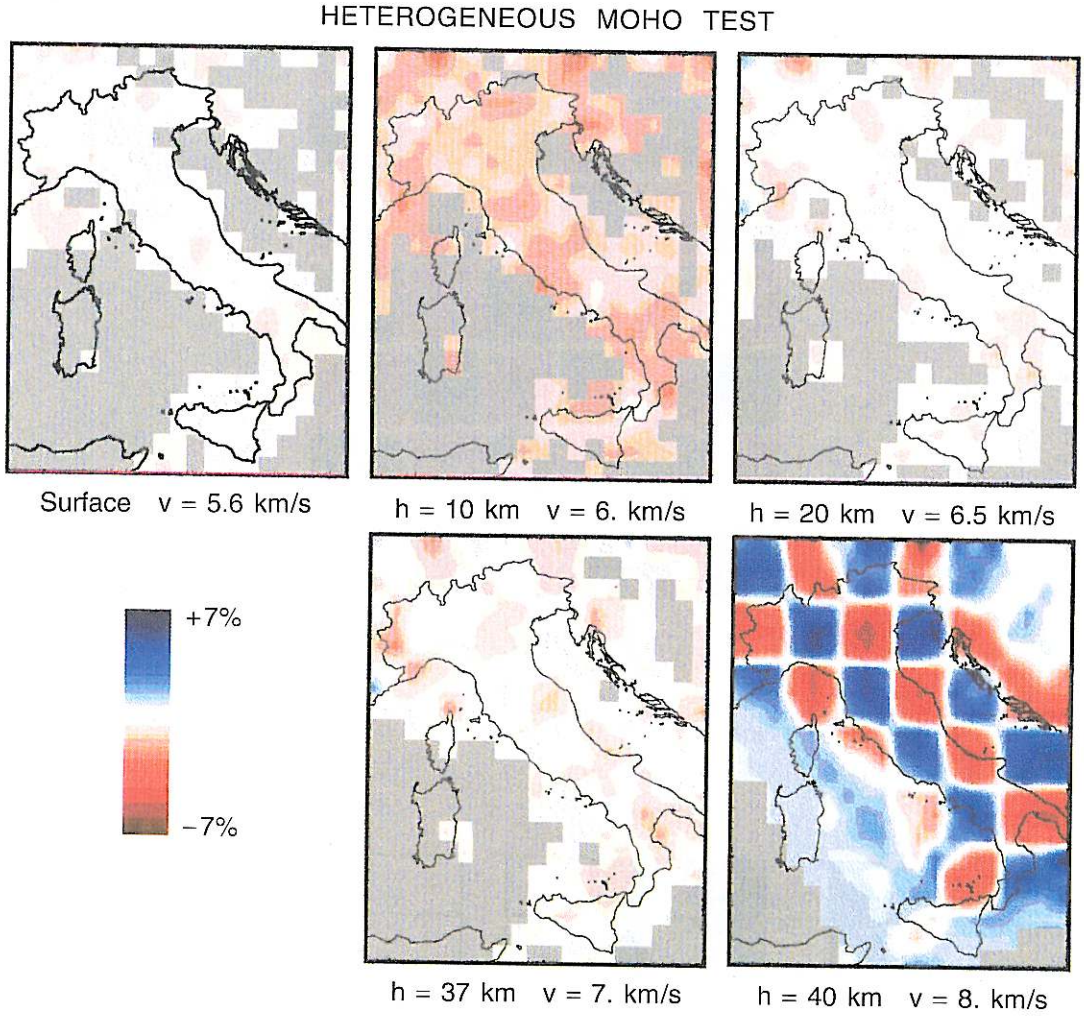

Fig. 9. Results of the inversion of synthetic data generated with S_m model at the surface, 10 km, 20 km, 37 km and 40 km. The mean velocity value for each layer are 5.6, 6.0, 6.5, 7.0 and 8.1 km/s respectively.

ance was evaluated from the *a posteriori* residuals. The resolution represents the interdependence among predicted model parameters.

The inversion of the actual data set was performed using two different grid sizes in order to verify the independence of the results from the node spacing. The diagonal elements of the resolution matrix obtained for the model 1 were lower than those obtained for model 2. Nevertheless the trace of the resolution matrix was 192 for model 1 and 128 for model 2. The data variance was almost the same for the two grid sizes: 0.645 s^2 and 0.644 s^2 at the fifth iteration.

We can conclude that the model obtained using the denser grid has higher quality than the other one.

Toomey and Foulger (1989) introduced the

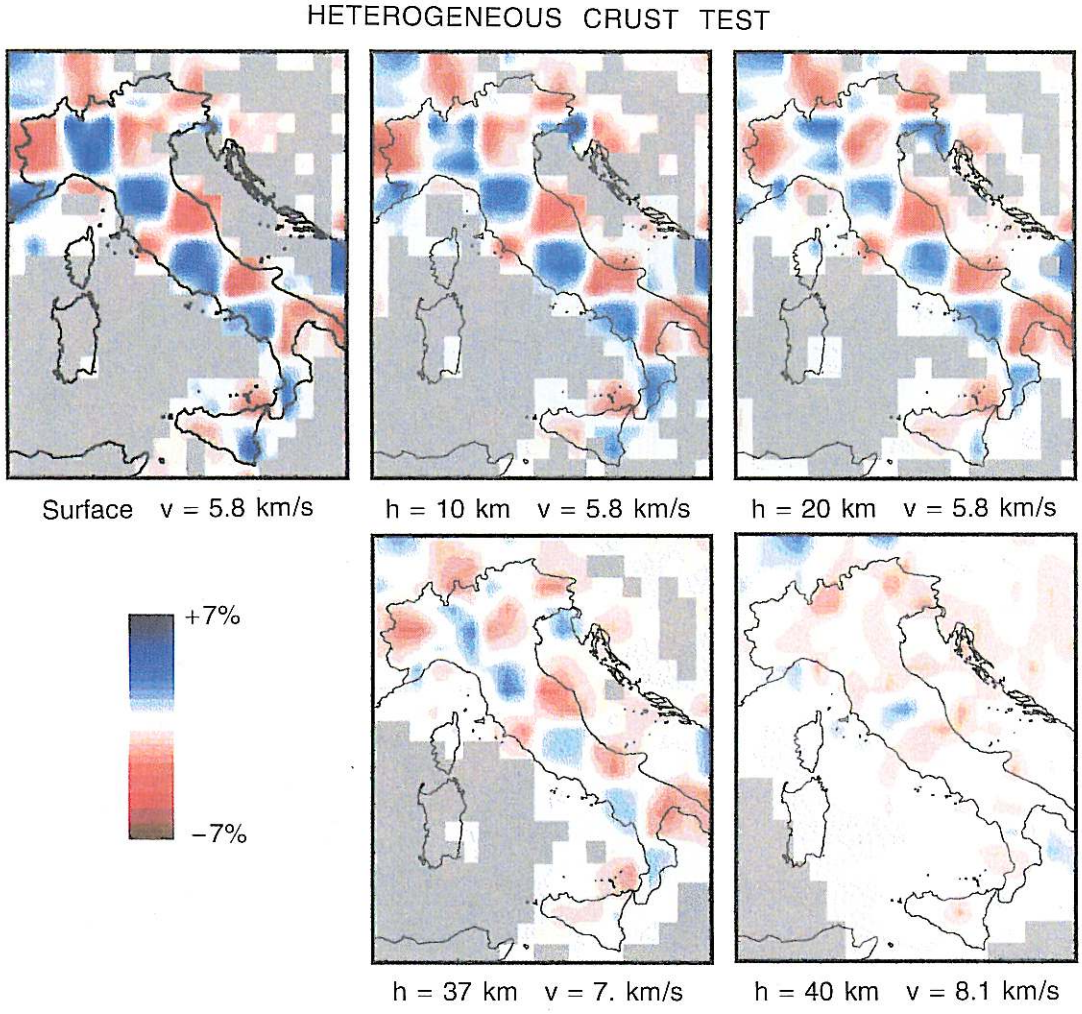

Fig. 10. Results of the inversion of synthetic data generated with S_c model. Depth of the layers and mean velocity are as in fig. 8a-c.

use of the Spread Function (Menke, 1984) to tomography as a single parameter that characterizes the model resolution in each node. We used the following formula for the Spread Function F_i of the i-th model parameter:

$$F_i = \frac{\sum_{j=1}^{N} d_{ji} R_{ji}^2}{\sum_{j=1}^{N} R_{ji}^2} \qquad (6.1)$$

here R_{ji} is an element of the resolution matrix, d_{ji} is a weighting factor defined as the distance between the j-th and i-th node and N is the number of parameters. The values of the Spread Function at the nodes can be easily plotted: figs. 11 and 12 show the maps of the Spread Function of the two models. In the ideal case in which the resolution matrix is an identity matrix (parameter not interdependent),

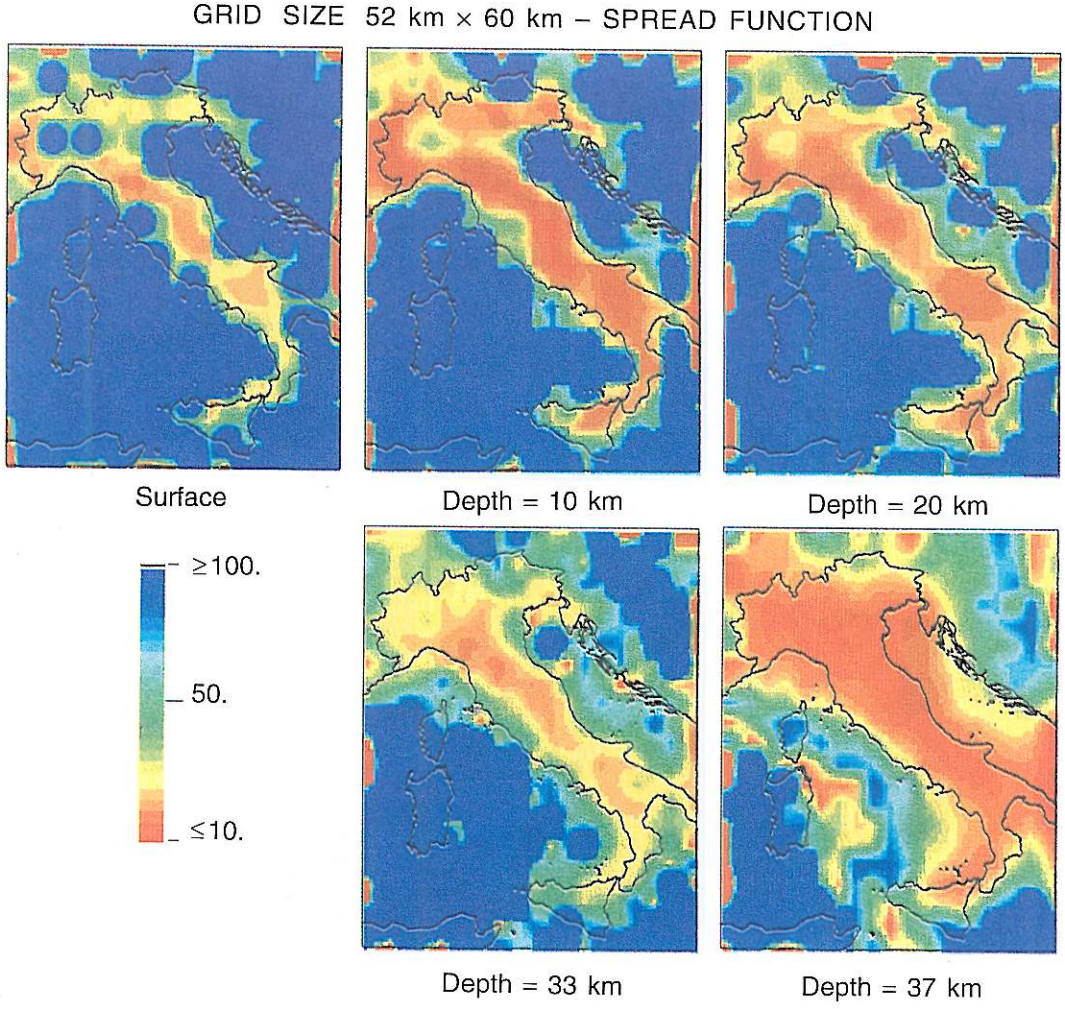

Fig. 11. Spread Function mapped at the surface, at 10 km, 20 km, 33 km and 37 km for the finer grid.

the Spread Function would be zero for all the parameters, while the more the non diagonal elements of the resolution matrix differ from zero, the larger the Spread Function would be. As a consequence we will have high resolution where the Spread Function has lower values.

The maps of the Spread Function at various layers confirm that the shallower crustal layers are less resolved than the deeper ones. Moreover the Tyrrhenian region is mostly not resolved. These conclusions are in agreement with those previously drawn in the synthetic test. Although the number of P_g and S_g arrival times were one third of the total, low values of the Spread Function are well recognizable in the peninsular region at about 10 and 20 km depth (see figs. 11 and 12).

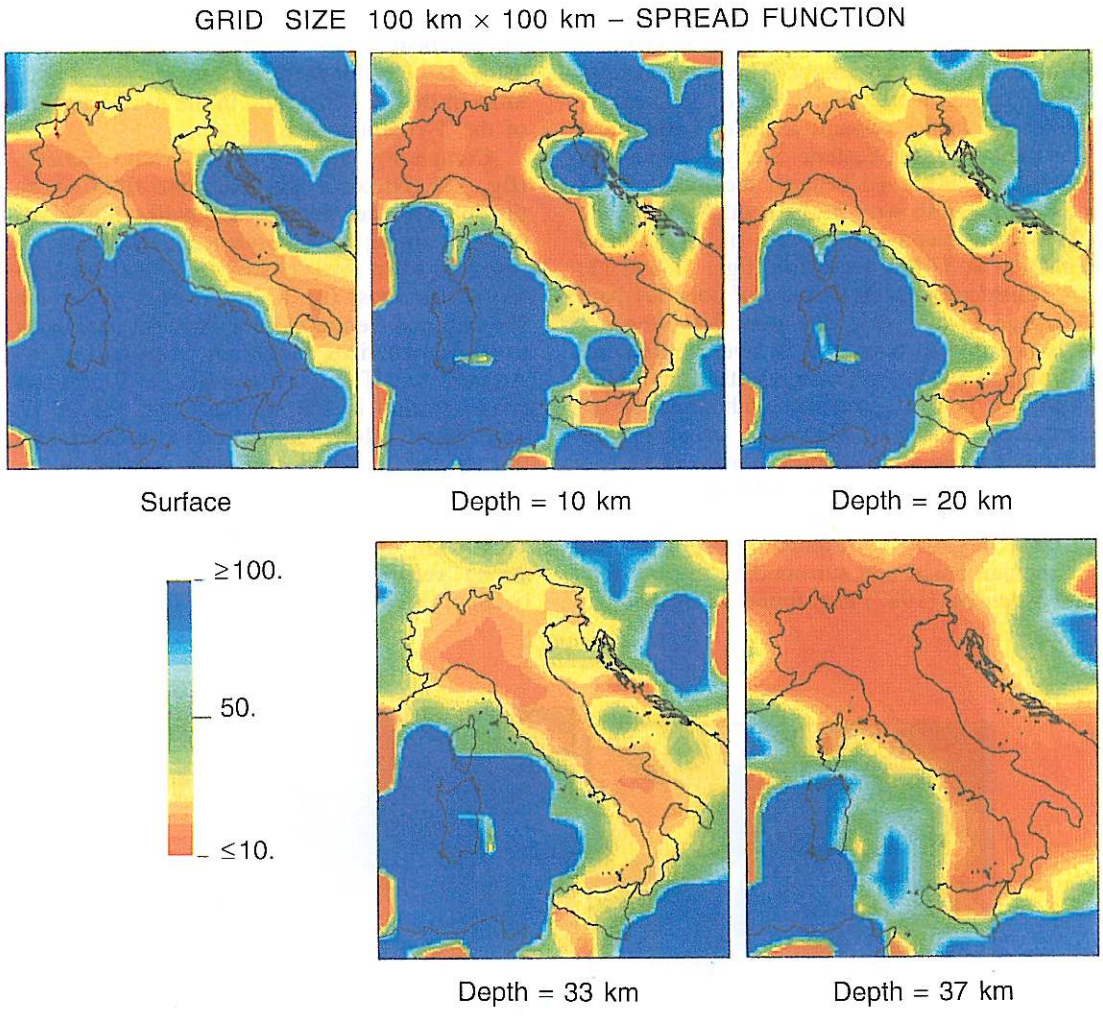

Fig. 12. Spread Function as in fig. 11 for the less dense grid.

7. Results

In this section the maps of the velocity adjustments at different depths are presented.

Similar trends can be observed in both models resulting from the inversions. Figures 13 to 17 show the maps of the velocity field at all depths, computed for both grid sizes after five iterations. The gray areas stay for non-inverted nodes; the red-blue scale corresponds to the velocity variations ranging from −7% to +7% with respect to the starting velocity value of the layer.

Wide positive anomalies can be observed at 37 km depth in the northern part of the Tyrrhenian Sea and from the Adriatic region westward to the Po Valley (fig. 13). The roots of the Western and Central Alps are characterized

by lower velocities. Low velocity anomalies are also found beneath the Tyrrhenian coast of Central and Southern Italy. This area extends from the thermally active zone of Tuscany southward to the volcanic areas of Latium and Campania up to Eastern Sicily. A positive anomaly is observed beneath the Ionian coast of the Calabrian Arc. In the central part of the Tyrrhenian basin the values of the Spread Function at 37 km depth (see figs. 11 and 12) are considerably high because of poor ray path coverage in east-west direction. Nevertheless, it is possible to point out an average velocity lower than 8.0 km/s. These results at the Moho depth are in full agreement with previous tomographic works of Mantovani *et al.* (1980) who evidenced a noticeable decrease of P_n and S_n velocities from the more stable regions, such as the Adriatic and southern forelands, to the instable regions corresponding to the low Tyrrhenian basin and surrounding areas. Mele and Valensise (1987) also found an increase in the P_n velocity in the north-east direction from the Tyrrhenian Sea to the Adriatic Basin. The same authors obtained velocity greater than 8 km/s in the Po Valley and in the northern coast of the Tyrrhenian Sea.

Comparing the map of the Moho isobaths (fig. 18) (Nicolich and Dal Piaz, 1990) with the map of the velocity anomalies at 37 km depth, a strong correspondence is easily recognized between low velocity trend and thickening of the crust (up to 40-50 km), under the Western and Central Alpine Arc. An analogous trend characterizes the Dinaric Alps east of the Adriatic Sea. The crust beneath the Tyrrhenian coasts is thin in the southern part (about 15 km), where a low velocity belt is located, and thicker eastward underneath the peninsula.

Figure 14 shows the velocity field of the model at the top of the fourth layer (33 km). This 4 km thick layer was set to introduce a strong velocity gradient needed for the ray bending at Moho depth. For this layer, the

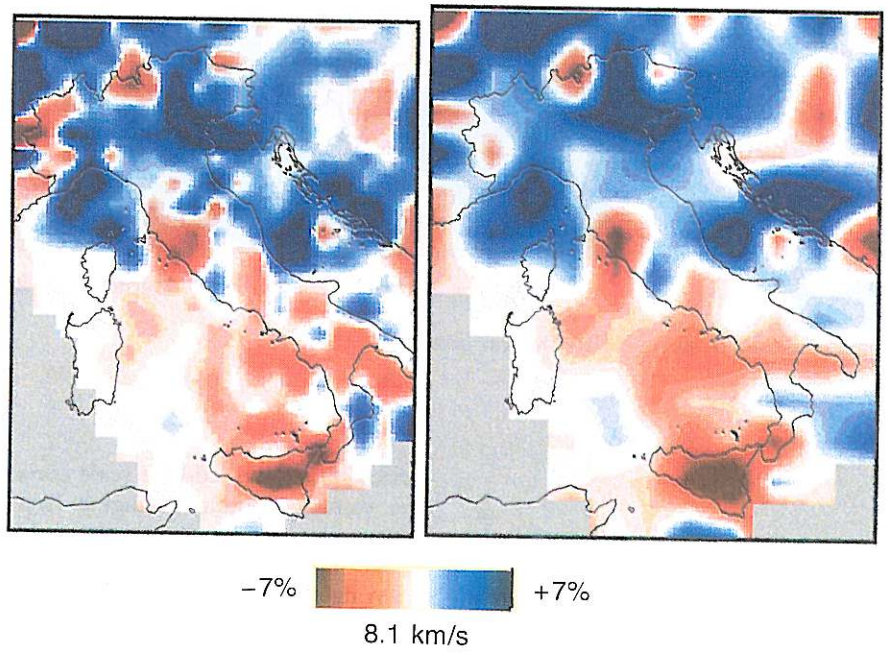

Fig. 13. Velocity adjustments at 37 km of depth for the finer grid (left) and less dense grid (right); variations between +7% and −7% are reported. The mean velocity of this layer is 8.1 km/s.

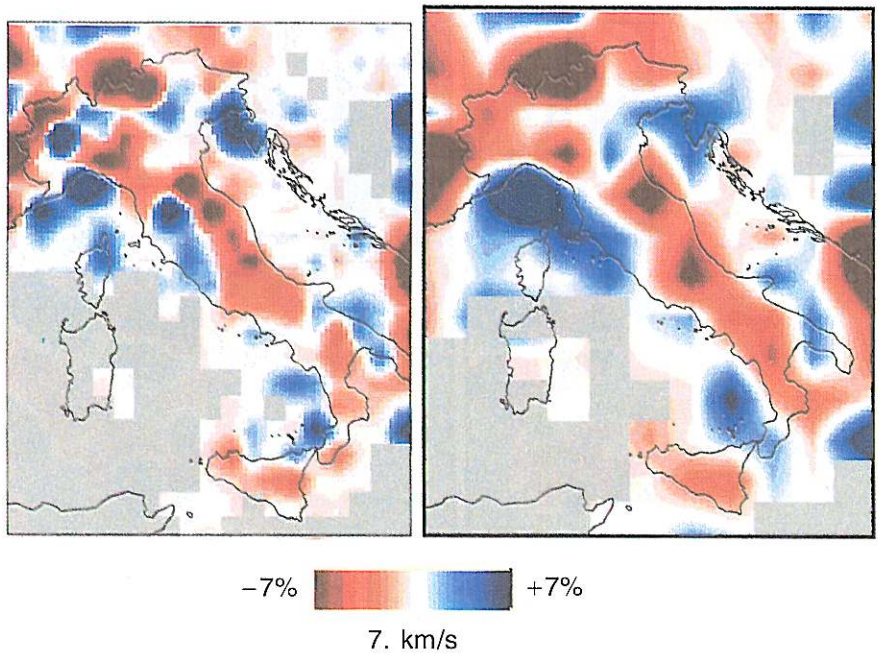

Fig. 14. Velocity adjustments at 33 km of depth as in fig. 13. The mean velocity of this layer is 7.0 km/s.

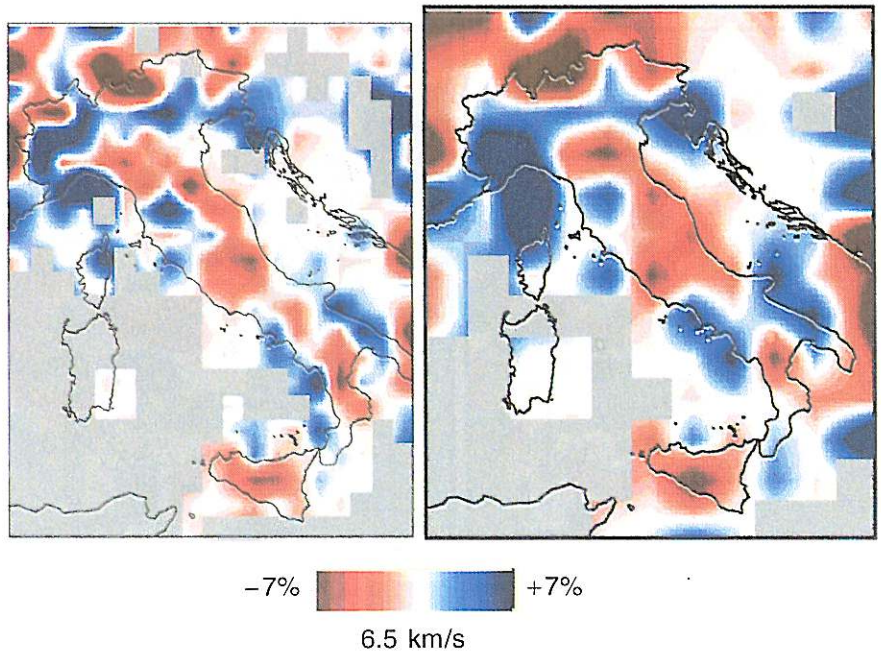

Fig. 15. Velocity adjustments at 20 km of depth as in fig. 13. The mean velocity of this layer is 6.5 km/s.

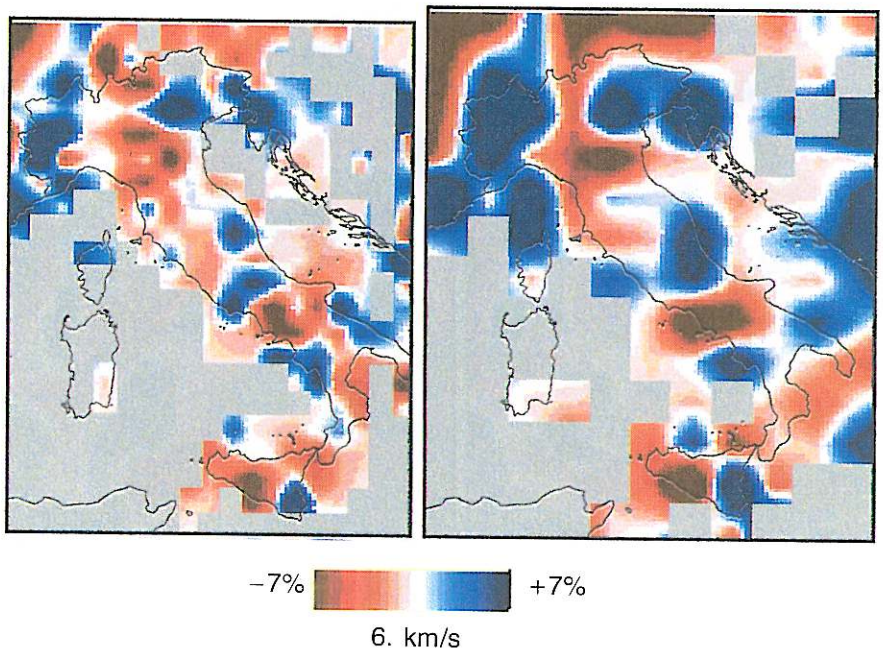

Fig. 16. Velocity adjustments at 10 km of depth as in fig. 13. The mean velocity of this layer is 6 km/s.

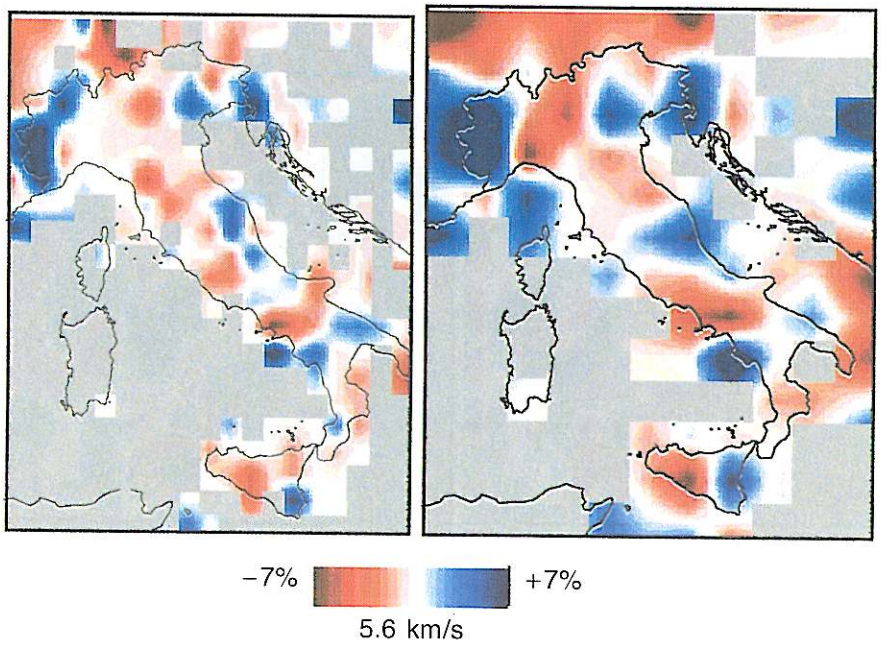

Fig. 17. Velocity adjustments at the surface as in fig. 13. The mean velocity of this layer is 5.6 km/s.

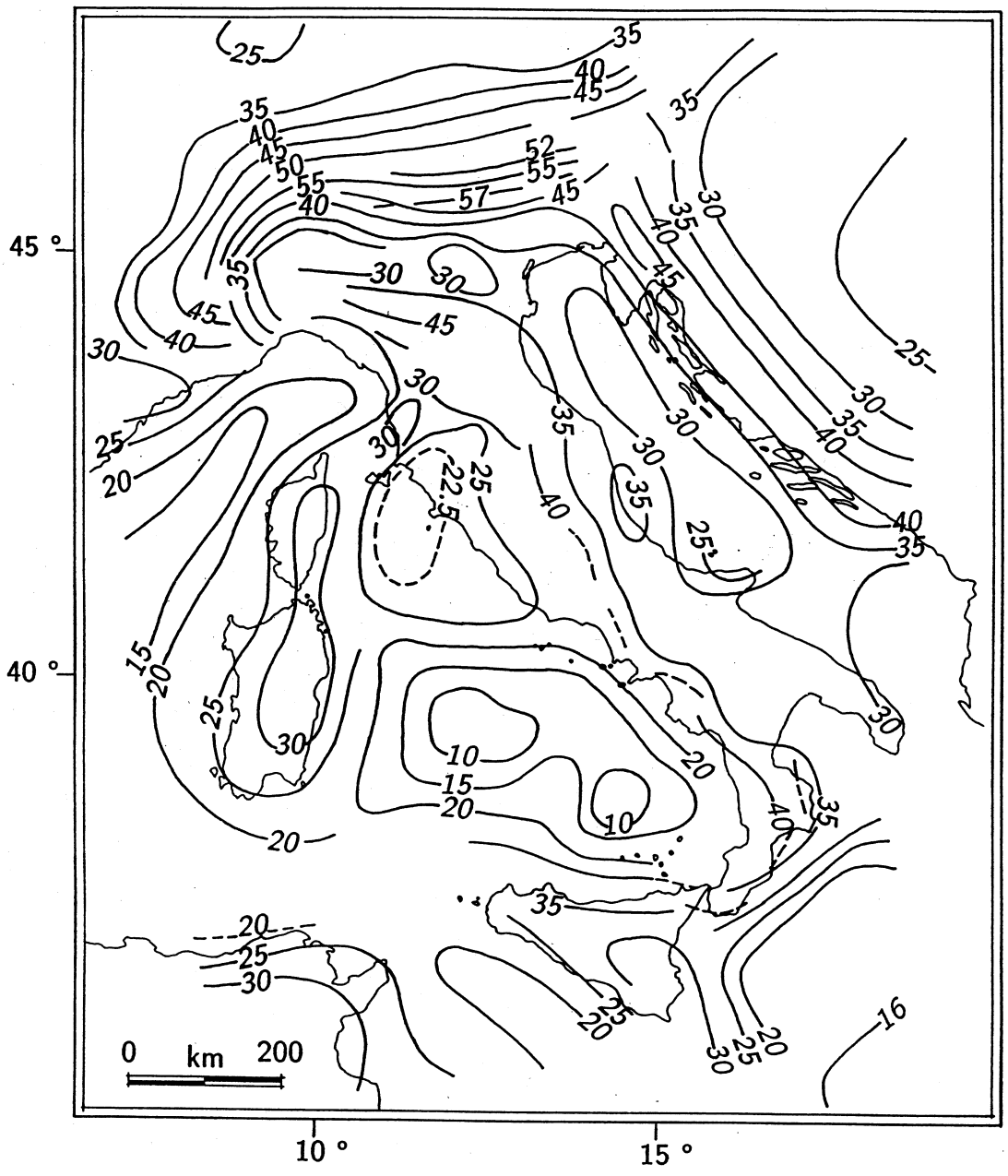

Fig. 18. Map of the isobaths of the Moho underneath the Italian region (after Nicolich and Dal Piaz, 1990).

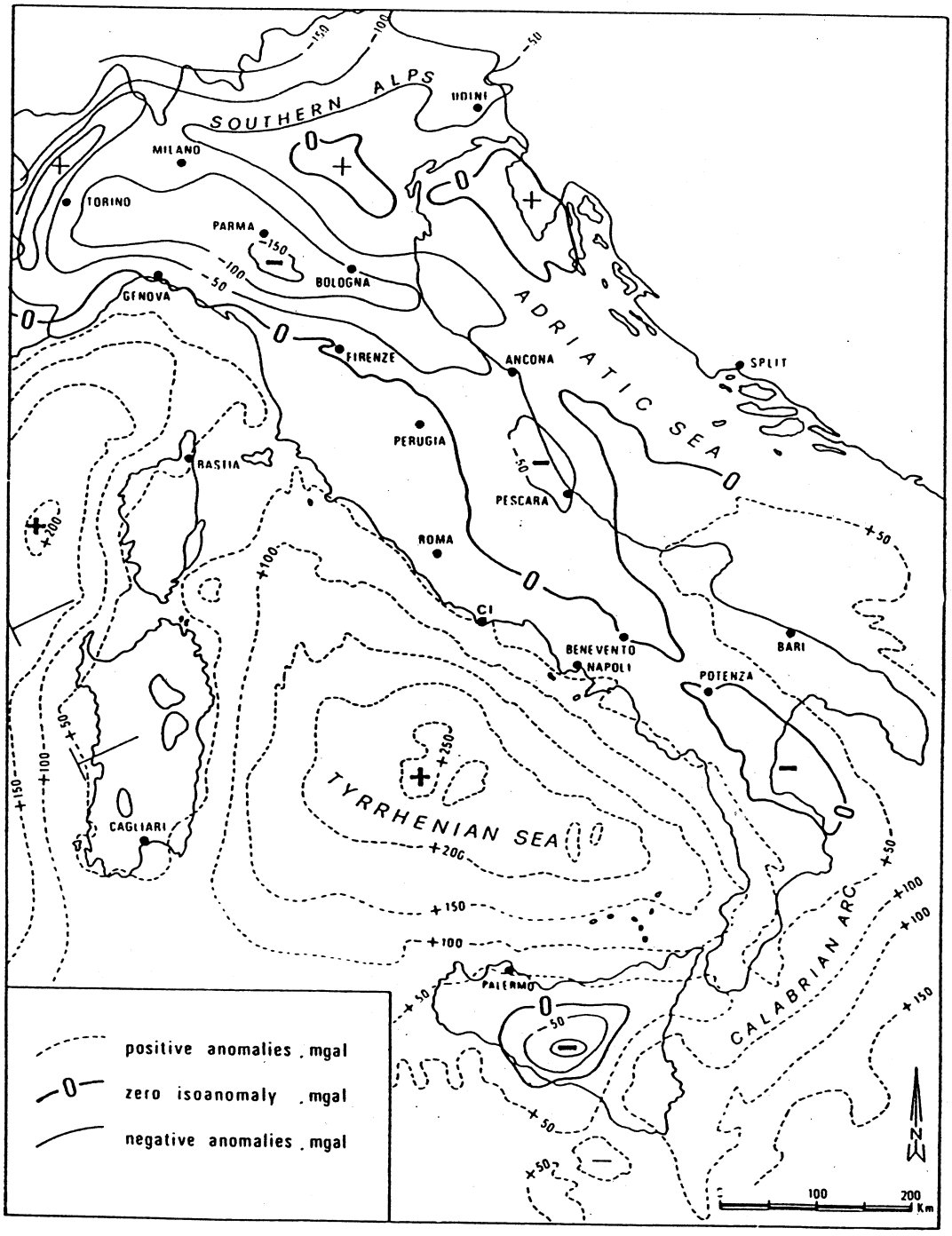

Fig. 19. Contour map of the Bouguer anomalies for the Italian region (after Lavecchia, 1988, modified).

Spread Function reveals a good resolution only in restricted peninsular zones; this is due both to the short permanence inside the layer and to the almost vertical direction of the ray paths. The velocity field at the top of the third layer (20 km) is shown in fig. 15. The extension of the non-inverted region is remarkable beneath Tyrrhenian Sea, Sardinia and limited zones of the Northern Adriatic Sea.

The resolved areas show a high-velocity trend underneath the Northern Tyrrhenian Sea and Western Alps. A significant velocity contrast extends from Eastern Sicily to the Calabrian Arc. The Apenninic chain is characterized by low velocity in its northern and central parts; in the southern part we observe high velocity anomalies in Campania and in the Adriatic coast.

The velocity field at 10 km depth is reported in fig. 16. The shape and the extension of the resolved area is strongly determined by the location of the receivers. A velocity contrast characterizes the central Apennines. The high velocity values observed in the Western Alps at 20 km of depth still persist in this layer.

At the surface the Spread Function reaches high values almost everywhere and a good resolution is restricted to the Central Apennines and Western Alps only (fig. 17). These two areas are characterized by small velocity contrast and high velocity respectively. The high velocity anomaly in the Western Alps is the only feature extending in all the crustal layers.

The Bouguer anomalies depicted in fig. 19 (Lavecchia, 1988) show positive values (plus signes) mainly west of the Apennine ridge and in restricted areas of Northern Italy. These positive gravity anomalies correspond to positive velocity adjustments in the crustal layers of North-Western and North-Eastern Italy. In particular the evident positive velocity anomaly in the crustal layers beneath the Western Alps might correspond to the so called *Ivrea body*, generally interpreted as a possible segment of the Adriatic microplate intruded in the crust (Laubscher, 1988). The negative Bouguer anomaly beneath the Po Valley extends where crustal low velocity anomalies is observed. A large negative gravity anomaly centered in Sicily corresponding with a crustal low velocity one, represents another remarkable feature.

8. Conclusions

Caution must be exercised when interpreting the velocity maps because of the possible bias between poor modelling of the crustal thickness and velocity found at the Moho. Nevertheless the method proposed by Pavlis and Booker and modified by Thurber helps to point out some main features of the velocity gradient in the uppermost mantle of the Italian region.

The velocity field at Moho depth presents a velocity increase from the Tyrrhenian basin toward the Adriatic sea and Alpine chain. This can be ascribed to the higher stability of the Adriatic forelands and the Alpine region with respect to the Tyrrhenian basin. Close similarities are observed comparing the map of the velocity adjustments and the map of the Moho isobaths: velocity and thickening of the crust follow almost the same trends.

In the shallower crustal layers the persistence of a positive velocity anomaly in the Western Alps is observed.

The large Tyrrhenian Sea region is insufficiently resolved almost at all depths because of the poor network coverage of Corsica and Sardinia and the resulting lack of ray paths in the east-west direction. Although these regions are characterized by an almost inexistent seismic activity, the installation of seismological stations would make a relevant contribution to the tomographic analysis of the Tyrrhenian Sea area.

The application of inversion techniques to smaller areas, where local network data are available, can improve the details of the models in the upper crust. However, a limited extension of the analysed area would reduce the number of P_n ray paths and consequently prevent a good resolution at Moho depth.

Acknowledgements

We are very grateful to William Prothero for providing the algorithm that computes the two-point ray tracing. Thanks are due to Ornella Bonamassa, Gianluca Valensise and John Vidale for carefully reading the manuscript and for many suggestions. We also thank Daniela Riposati for help in drafting.

REFERENCES

AKI, K., A. CHRISTOFFERSON and E.S. HUSEBYE (1977): Determination of the three-dimensional seismic structure of the lithosphere, *J. Geophys. Res.*, **82**, 277-296.

AMATO, A., R. DE FRANCO and L. MALAGNINI (1990): Local source tomography: applications to Italian areas, *Terra Nova*, **2**, 596-608.

AMATO, A., G.B. CIMINI and B. ALESSANDRINI (1991): Struttura del sistema litosfera-astenosfera nell'Appennino Settentrionale da dati di tomografia sismica, *Studi Geologici Camerti, special issue*, **1**, 83-90.

AMATO, A., B. ALESSANDRINI and G.B. CIMINI (1993): *P*-wave tomography of Italy, in *Seismic Tomography* edited by H.M. IYER and K. HIRAHARA (Chapman and Hall, London), 361-397.

BABUŠKA, V., J. PLOMEROVÁ and J. ŠILENÝ (1984a): Large-scale oriented structures in the subcrustal lithosphere of Central Europe, *Ann. Geophys.*, **2**, 649-662.

BABUŠKA, V., J. PLOMEROVÁ and J. ŠILENÝ (1984b): Spatial variations of *P* residuals and deep structure of the European lithosphere, *Geophys. J. R. Astron. Soc.*, **79**, 363-383.

BULAND, R. (1976): The mechanics of locating earthquakes, *Bull. Seismol. Soc Am.*, **66**, 173-187.

CALCAGNILE, G. and G.F. PANZA (1981): The main characteristics of the lithosphere-astenosphere system in Italy and surrounding regions, *PAGEOPH*, **119**, 865-879.

CASSINIS, R. (1983): Seismicity and crustal structure in the Italian region: a preliminary zoning, *Boll. Geofis. Teor. Appl.*, **25**, 3-26.

CASSINIS, R. and A. RANZONI (1987): Contribution of controlled source seismology to the study of seismogenesis: examples from the Italian transitional area, *Tectonophysics*, **140**, 81-91.

ELLSWORTH, W.L. and R.Y. KOYANAGI (1977): Three-dimensional crust and mantle structure of Kilauea Volcano, Hawaii, *J. Geophys. Res.*, **82**, 5379-5394.

EVANS, J.R. (1986): *Teleseismic Travel Time Residual Analysis System: a User's Manual*, U.S. Geological Survey.

KLEIN, F.W. (1978): Hypocenter location program HYPOINVERSE: users guide to versions 1, 2, 3 and 4. U.S. Geol. Surv., *Open-File Rept.*, **78**, 694, 1-113.

LAUBSCHER, H.P. (1988): The arcs of the Alps and the Northern Apennines: an updated view, *Tectonophysics*, **146**, 67-78.

LAVECCHIA, G. (1988): The Tyrrhenian-Apennines system: structural setting and seismotectogenesis, *Tectonophysics*, **147**, 263-296.

MANTOVANI, E., F. FARSI and D. BABBUCCI (1980): Body wave velocities and lateral heterogeneity in the Italian region, *Boll. Geofis. Teor. Appl.*, **22**, 211-221.

MANTOVANI, E. and E. BOSCHI (1982): Short period rayleigh wave dispersion in the Calabrian Arc and surrounding regions, *Earth Evolution Sciences*, **3**, 239-242.

MANTOVANI, E., G. NOLET and G.F. PANZA (1985): Lateral heterogeneity in the crust of the Italian region from regionalized Rayleigh-wave group velocities, *Annales Geophysicae*, **3** (4), 519-530.

MELE, F.M. and G. VALENSISE (1987): Un modello crostale per la localizzazione di eventi sismici regionali rilevati dalla Rete Sismica Nazionale Centralizzata dell'ING, in *Proceedings of the 6° Annual Meeting of the Gruppo Nazionale di Geofisica della Terra Solida*, Roma, Italy.

MENKE, W. (1984): *Geophysical Data Analysis* (Academic Press, London).

NELDER, J.A. and R. MEAD (1965): A simplex method for function minimization, *Computer J.*, **7**, 308.

NICOLICH, R. (1981): Crustal structures in Italian Peninsula and surrounding seas: a review of DDS data, in *Sedimentary Basin of Mediterranean Margins*, edited by F.C. WEZEL (Tectonoprint, Bologna), 3-17.

NICOLICH, R. (1989): Crustal structures from seismic studies in the frame of the European Geotraverse southern segment and CROP projects, in *The Lithosphere in Italy Advances in Earth Science Research*, edited by A. BORIANI *et al.* (Accademia Nazionale dei Lincei, Roma), 41-61.

NICOLICH, R. and R. DAL PIAZ (1990): Moho isobaths, in *Structural Model of Italy and Gravity Map, Sheet 2* (Consiglio Nazionale delle Ricerche).

PAVLIS, G.L. and J.R. BOOKER (1980): The mixed discrete-continuous inverse problem: application to the simultaneous determination of earthquake hypocenters and velocity structure, *J. Geophys. Res.*, **85**, 4801-4810.

PROTHERO, W.A., W.J. TAYLOR and J.A. EICKEMEYER (1988): A fast, two-point, three-dimensional raytracing algorithm using a simple step Search method, *Bull. Seismol. Soc. Amer.*, **78**, 1190-1198.

ROMANOWICZ, B.A. (1980): A study of large-scale lateral variations of *P* velocity in the upper mantle beneath Western Europe, *Geophys. J. R. Astron. Soc.*, **63**, 217-232.

SCARPA, R. (1982): Travel-time residuals and three-dimensional velocity structure of Italy, *Pure Applied Geophys.*, **120**, 583-606.

SPAKMAN, W. (1986): The upper mantle structure in the Central European-Mediterranean Region, in *European Geotraverse EGT Project, the Central Segment*, edited by R. FREEMAN, ST. MUELLER and P. GIESE (European Science Foundation, Strasbourg), 215-222.

SPAKMAN, W. (1990): Tomographic images of the upper

mantle below Central Europe and the Mediterranean, *Terra Nova*, **2**, 542-552.

THURBER, C.H. (1981): Earth structure and earthquake locations in the Coyote Lake area, Central California, *Ph. D. Thesis.*

THURBER, C.H. (1983): Earthquake locations and three-dimensional structure in the Coyote Lake area, Central California. *J. Geophys. Res.*, **88**, 8226-8236.

TOOMEY, D.R. and G.R. FOULGER (1989): Tomographic inversion of local earthquake data from the Hengill-Grensdalur Central Volcano Complex, Iceland, *J. Geophys. Res.*, **94**, 17497-17510.

(received October 18, 1994;
accepted March 20, 1995)